EiDA: A LOSSLESS APPROACH FOR THE DYNAMIC ANALYSIS OF CONNECTIVITY PATTERNS IN SIGNALS; APPLICATION TO RESTING STATE fMRI OF A MODEL OF AGEING

Giuseppe de Alteriis[1,*,**], **Eilidh MacNicol**[1,*], **Fran Hancock**[1], **Diana Cash**[1], **Paul Expert**[2], **Federico E. Turkheimer**[1]
[1]Department of Neuroimaging, Institute of Psychiatry, Psychology and Neuroscience, King's College London, London, UK
[2]Global Business School for Health, University College London, London WC1E 6BT, UK

[**]Corresponding author: Giuseppe de Alteriis; giuseppe.de_alteriis@kcl.ac.uk
[*]These authors contributed equally to this work.

ABSTRACT

Complexity science offers a framework for analysing high-dimensional, non-linear interacting systems such as financial markets or activity in the brain, to extract meaningful dynamic information for decision-making or scientific enquiry. By virtue of the data involved, various analytical methods are required for dimensionality reduction, clustering, discrete analysis, continuous flow analysis, and for estimations of complexity.

We introduce EiDA (Eigenvector Dynamic Analysis), a closed form analytical methodology to losslessly extract dynamical functional connectivity (dFC) information from instantaneous phase-locking matrices ($\mathbf{iPL}$). EiDA builds on the existing LEiDA approach (Leading Eigenvector Dynamic Analysis), by showing that the $\mathbf{iPL}$ matrix is of rank 2, and can thus be completely characterised by two eigenvectors. We give a full analytical derivation of the eigenvectors and their associated eigenvalues. As a second step we propose two alternatives to analyze the time evolution of the $\mathbf{iPL}$ matrix or equivalently of instantaneous connectivity patterns: i) Discrete EiDA, which identifies a discrete set of phase locking states using k-means clustering on the decomposed $\mathbf{iPL}$ matrices, and ii) Continuous EiDA, which introduces a 2-dimensional position and reconfiguration speed representation of the eigenvectors. In Continuous EiDA, dynamic Functional Connectivity is conceived as a continuous exploration of this 2-D space. Finally, we show that the two non-trivial eigenvalues are interdependent as their sum is equal to the number of signal channels, and define spectral metastability as the standard deviation of the the spectral radius, the first eigenvalue. Finally, we compute informational complexity using the Lempel-Ziv-Welch algorithm.

We apply EiDA to a dataset comprising a cohort of *M=48* rats among *N=44* brain regions, scanned with functional magnetic resonance imaging (fMRI) at *T=4* stages during a study of ageing. We previously found that static functional connectivity declined with age. In dFC, we found that using only the leading eigenvector resulted in the loss of dFC information, and that this was exacerbated with ageing. Additionally, we found that while k-means clustering did not yield satisfactory partitioning, continuous EiDA provided a marker for ageing. Specifically we found that reconfiguration speed of the first eigenvector increased significantly over the life-span concurrent with a reduction in spectral metastability. In addition, we found an increase in informational complexity with age, and that this complexity was highly, significantly and inversely correlated ($R = 0.95$, $p < 0.001$) with the magnitude of the first eigenvalue of the $\mathbf{iPL}$ matrix. Finally, the computation time for EiDA outperforms numerical spectral decomposition algorithms: 2 orders of magnitude faster for 100x100 matrices, and 3 orders of magnitude faster for 10,000x10,000 matrices.

EiDA provides an analytically principled method to extract connectivity (relationship) information without loss from high-dimensional time-series, establishes a link between dynamical systems and information complexity in resting-state neuroimaging, and significantly reduces computational time for high-dimensional data.

Keywords Ageing · fMRI · Dynamic Functional Connectivity

1 Introduction

The brain is now recognized as a complex dynamic system ((1; 2; 3; 4)) whose activity is best characterized by patterns of interaction across its constituents at different scales, e.g. molecular, cellular, systemic, ((5)). For this reason, dynamic functional connectivity (dFC) has become a major field of interest in the analysis of brain recordings ((6; 7)), may they be extracted from functional MRI (fMRI) or electrophysiological recordings, for the characterization of brain activity in health or disease. dFC is a development of the study of functional connectivity (FC) ((8)), which aims at quantifying the connectivity of signals in a functional sense, i.e., where the connections are not anatomically informed, but based on a measure of the similarity of signals across the whole acquisition ((9; 10)). However, if FC is "static", in the sense that it computes connectivity measures which are representative of the whole recordings,for example using Pearson Correlation or Mutual Information, dFC instead attempts to characterize the time evolution of the connectivity patterns of brain activity ((6; 7; 11; 12; 13)).

In doing so, any dFC approach faces at least two problems: first is the choice of window size observation for the connectivity metric of interest. Let us suppose, for example, that we want to perform a dFC analysis of N signals by defining a time window size and computing correlation matrices within that window, see (14) for the limits of this approach. What would be the ideal window size and what would be an optimal (heuristic or theoretical) way to find it? The second problem is dimensionality: in the previous example, we would deal with the time evolution of an $N \times N$ matrix, which is not necessarily symmetric, and whose evolution over time might not be easily analyzed nor stored losslessly.

A powerful and well-established approach for dFC that overcomes both the problems of dimensionality and of time resolution stated above, is called Leading Eigenvector Dynamic Analysis (LEiDA) ((15)). LEiDA proposes to use the Hilbert transform of the time-series to recover the analytical signal ((16; 17)). This is a complex number defined for each acquisition time with an instantaneous amplitude and a phase. Therefore, for each pair of signals, it is possible to measure their relative phase ((18)), a measure often used to define "phase-locking" or synchronisation patterns. LEiDA introduces an instantaneous Phase Locking Matrix ($\mathbf{iPL}$) which contains, for each pair of signals, the phase difference (e.g. phase locking) at a each time step. This matrix is then decomposed into its orthogonal components, its eigenvectors, selecting only the first one and discarding the remaining eigenvectors, thus reducing dimensionality from $N \times N$ to N dimensions. To interpret the time evolution of this eigenvector, LEiDA then proposes to perform a clustering of the eigenvector time-series in order to identify discrete brain "states", e.g. connectivity patterns that are consistently explored by the brain during the data recording, as also proposed by (19). LEiDA has been applied with significant impact to study sleep-wake transition ((20)), psychedelics ((21; 22)), neurodevelopment ((23)), schizophrenia ((24)), and depression ((25; 26)).

Using the LEiDA approach, different synthetic dynamic indices of connectivity have been proposed such as the dwell time of states (average duration of uninterrupted exploration of a cluster), or the fractional occurrence (the total occurrence of a cluster as a percentage of the full recording). In addition, within states, it is possible to define measures capturing ideas drawn from complex systems theory such as metastability (a metric reflecting simultaneous tendencies for coupling and decoupling) ((27; 28; 29; 4)).

In this paper we question and explore two additional aspects of the LEiDA approach to define EiDA (Eigenvector Dynamic Analysis). First, it has been reported that the first eigenvector explains >50% of the variability in the iPL matrix (30). We therefore decided to investigate, in detail, the extent of information loss when only the leading eigenvector is considered, and to develop a closed form analytical approach that retains the complete information from the decomposition. Second, we investigate whether in certain circumstances it may be more appropriate to model dynamic connectivity as a smooth transition across configurations ((31)), instead of identifying, through clustering, discrete and separate brain states.

In doing so, we identify the $\mathbf{iPL}$ matrix and its evolution as the most important and informative dFC object. Given its particular structure, it is always possible to decompose the matrix analytically into two eigenvectors. This decomposition provides the theoretical background for LEiDA-based dynamic functional connectivity studies. Eigenvector decomposition allows the compression of the $N \times N$ $\mathbf{iPL}$ matrix into just $2N$ elements without loss and, furthermore, using the analytical form of the two eigenvectors drastically reduces the computation times of the eigendecomposition

(up to 1000x). We further demonstrate how the evolution of the two eigenvectors can be used to quantify the trajectories of the dynamic connectivity patterns. We use both a discrete state approach, using clustering of both the eigenvectors as in LEiDA, which we call Discrete EiDA but also a continuous flow analysis using a 2-dimensional embedding, which we call Continuous EiDA. Together with EiDA, we propose two theoretically informed measures of phase locking based on the norm of the $\mathbf{iPL}$ matrix, namely the spectral radius and spectral metastability.

As an exemplar application of EiDA, we consider a longitudinal fMRI data-set acquired across the life-span of a cohort of rodents (four data-sets) (32; 33). This is a controlled experimental setting that challenges the methodology to recover the trajectories of expected loss of dynamical connectivity associated with ageing (31; 34; 35; 36; 37; 38; 39; 40; 41).

2 Materials and Methods

A summary of our approach is outlined in Figure 1

We define a "recording" as the collection of N signals $x_1(t), x_2(t), ..., x_N(t),\ t = 1, \ldots, T$. We refer to a "group" as a set of recordings. In our case, as detailed in 2.9, the recordings are resting-state fMRI signals obtained during a two year study of brain ageing in rodents where the time-series in each acquisition were obtained from the parcellation of $N = 44$ anatomical brain regions ((32; 33)). The acquisitions were repeated for each animal four times during the life-span of the study. The study is described in section 2.9.

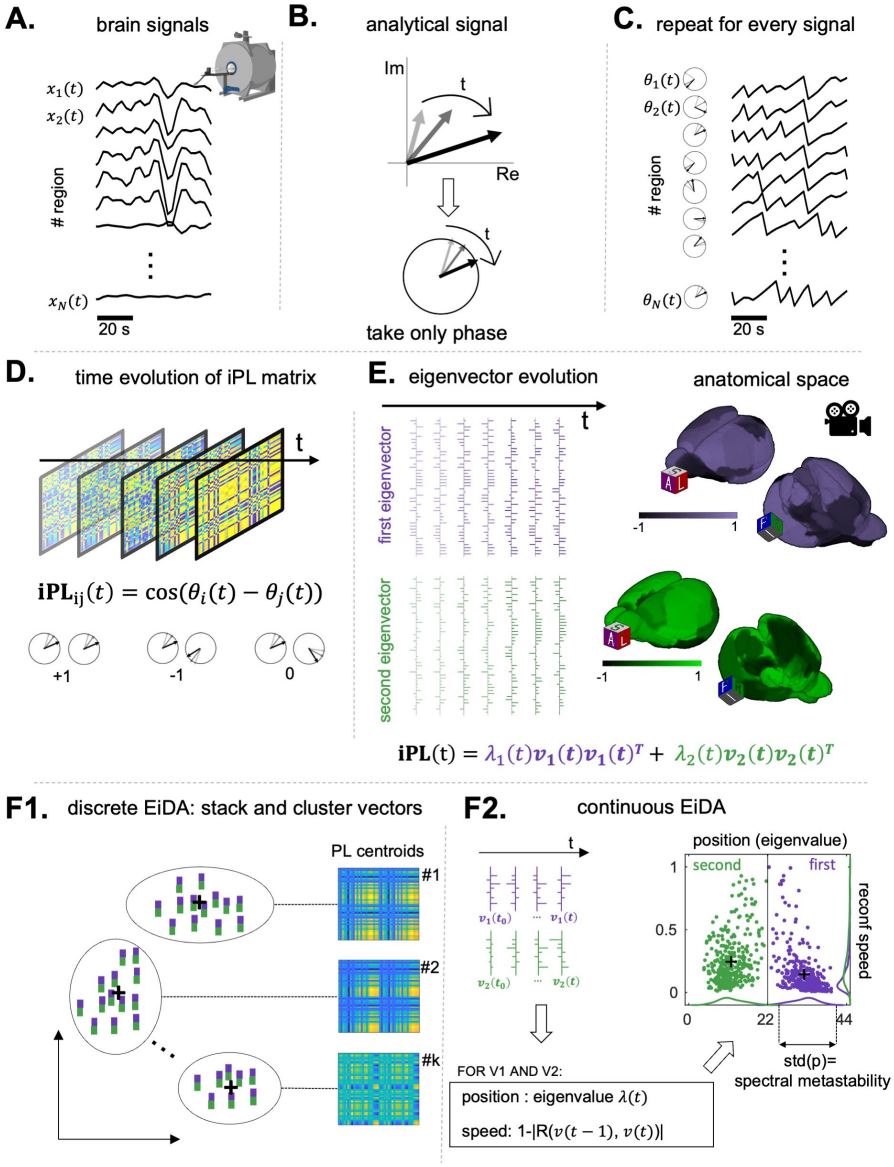

$$\mathbf{iPL}_{ij}(t) = \cos(\theta_i(t) - \theta_j(t))$$

$$\mathbf{iPL}(t) = \lambda_1(t)\boldsymbol{v_1}(t)\boldsymbol{v_1}(t)^T + \lambda_2(t)\boldsymbol{v_2}(t)\boldsymbol{v_2}(t)^T$$

Figure 1: Summary of the proposed method. We consider rat fMRI time-series but the method is applicable to any source of signals. **A**. We start from a multi-dimensional timeseries: the fMRI signals from 44 rat brain areas. **B**. For each signal, we compute its analytical representation via Hilbert Transform obtaining a complex number that evolves in time, of which we consider only the phase. **C**. We repeat this procedure for every signal to obtain a multi-dimensional timeseries of phases. **D**. At each time step, we compute the instantaneous Phase Locking Matrix (**iPL**), obtaining a time-series of matrices. The entry i, j of the matrix is the cosine of the difference of the phases i and j. If they are equal, it will be 1, -1 if opposite and 0 if they are in quadrature. **E**. The matrix being of rank 2, see methods, we decompose into its two non trivial eigenvectors, therefore reducing the data to a timeseries of two vectors evolving over time. Note that at each time t, the eigenvectors can be projected back in the anatomical space, as they have the same dimensionality of the timeseries. **F**. Once we obtain the timeseries of eigenvectors for each recording, we propose two alternative analysis strategies. *F1*. Discrete EiDA stacks the two eigenvectors in a single array and performs k-means clustering to identify k states. *F2*. Continuous EiDA, on the other hand, embeds the flow of eigenvectors in a 2D position-speed space. The first dimension is the eigenvalue relative to the eigenvector, which is called position, because it is the norm of the iPL matrix. The second one is the speed at which eigenvectors evolve, the reconfiguration speed, which is inversely proportional to the correlation between adjacent eigenvectors: the more two eigenvectors are correlated in time, the slower they are evolving.

2.1 Static Analysis of recordings and Static Functional Connectivity

We used static connectivity measures, i.e. computed over the whole recording duration, ((42; 43)), as a benchmark and point of reference for the dynamic investigations of the recordings. The simplest measure we considered is the Matrix of Pearson Correlations of signals. For each recording we defined a single matrix $\mathbf{P}$, where $\mathbf{P}_{ij} = \mathrm{R}(x_i, x_j)$, and R(.,.) is the Pearson correlation coefficient between two signals. In order to obtain an overall inter-subject connectivity matrix for each of the four groups of recordings, we averaged the squared Pearson correlation coefficients values in each group, therefore obtaining four average correlation matrices, to show the effect of ageing in the static correlation patterns. We calculated the squared values to take into account, in the averaging process across individuals, of both positive and negative correlations. Moreover, we defined used the matrix Frobenius norm, the sum of the squared values of the matrix ((44)), as a synthetic measure of overall connectivity for a single recording.

As already mentioned in the introduction, however, connectivity patterns may not be stationary over time. This means that the "static" connectivity matrix may not convey all the information about the dynamics of the connectivity patterns over time ((14; 45)). We define then the **iPL** Matrix.

2.2 iPL Matrix

To perform a dynamic analysis and avoid the need to define time windows, one needs an instantaneous measure that can be used to compute the level of functional connectivity between each pair of brain regions. A common approach to this task is to obtain an analytical representation of a signal, which expresses a time series as a complex number, and thus an instantaneous amplitude $A(t)$ and instantaneous phase $\theta(t)$. To compute the analytical signal, we use the Hilbert transform. The analytical form of a signal $x(t)$ is equal to $x(t) + i\mathcal{H}\{x(t)\}$, where $\mathcal{H}\{x(t)\}$ is the Hilbert transform of the signal. The Hilbert transform of a signal is defined as:

$$\mathcal{H}\{x(t)\} = \frac{1}{\pi}\mathrm{p.v.}\int_{-\infty}^{\infty}\frac{x(t)}{t-\tau}\,d\tau \tag{1}$$

For more details about the Hilbert transform, please see ((18; 46)). To provide a visual illustration, (see Figure 1), we can conceive the analytical signal as a "clock" with the hand of the clock that changes length over time (with the amplitude $A(t)$) and rotates (changes with phase $\theta(t)$).

Therefore, at each time instant t, one could ask whether two signals are "phase locked", i.e., they have the same instantaneous phase $\theta(t)$: in this case the two hands of the two clocks point in the same direction, (see Figure 1, C,D). This can be done for each pair of signals, and at each time point. We can thus define an "instantaneous" phase locking value $\mathbf{ipl}(\mathbf{t})_{\mathbf{1,2}}$ between two signals $x_1(t)$ and $x_2(t)$ as the cosine of the difference of two phases $\mathbf{ipl}(\mathbf{t})_{\mathbf{1,2}} = \cos(\theta_1(t) - \theta_2(t))$ ((18; 29; 15; 25; 26; 47; 27)). This value is equal to 1 if signals are perfectly in phase, -1 if their phase difference is π, and 0 if their phase difference is $\pm\frac{\pi}{2}$, i.e. the signals are in quadrature.

It is therefore possible to define, given N signals $x_1(t), x_2(t), ...x_N(t)$, an instantaneous Phase Locking Matrix, **iPL** Matrix, i.e. a matrix where $\mathbf{iPL}_{ij}(t) = \cos(\theta_i(t) - \theta_j(t))$ ((29)):

$$\mathbf{iPL}(t) = \begin{bmatrix} \cos(\theta_1(t)-\theta_1(t)) & \cos(\theta_1(t)-\theta_2(t)) & \dots & \cos(\theta_1(t)-\theta_N(t)) \\ \vdots & \ddots & & \vdots \\ \cos(\theta_N(t)-\theta_1(t)) & \cos(\theta_N(t)-\theta_2(t)) & \dots & \cos(\theta_N(t)-\theta_N(t)) \end{bmatrix} \in \mathbb{R}^{N\times N} \tag{2}$$

The analysis of connectivity patterns over time is transposed to the analysis of the evolution of the **iPL** matrix over time.

To compare static and dynamic connectivity matrix we computed the average **iPL** matrix for each recording, and then we averaged the matrices in the groups as previously done with the Pearson correlation matrices in 2.1. We also took the Frobenius norm of the average **iPL** matrix per recording.

2.3 Analytical Computation of the Eigenvectors of iPL Matrix

Let us consider the N signals at a certain time t and their instantaneous phases, computed via Hilbert Transform, which form a vector $\overrightarrow{\theta}(t) = (\theta_1(t), \theta_2(t), \theta_3(t), ...\theta_N(t))^T \in \mathbb{R}^N$. From this vector, we define, as in the previous section, an instantaneous Phase Locking (**iPL**) matrix, which is in principle different for each time t. Let us now, for simplicity, consider a single time t, and call the matrix **iPL** by abuse of notation, but remembering that the $\overrightarrow{\theta}$ vector changes at every time t and so does the matrix. Hence, the next procedure can be repeated at each time t.

Given that the matrix $\mathbf{iPL}_{ij} = \cos(\theta_i - \theta_j)$, and given that $\cos(x-y) = \cos(x)\cos(y) + \sin(x)\sin(y)$, then $\mathbf{iPL}_{ij} = \cos(\theta_i)\cos(\theta_j) + \sin(\theta_i)\sin(\theta_j)$. This means that the iPL matrix can be decomposed in the sum of two matrices:

$$\mathbf{iPL} = \begin{bmatrix} \cos(\theta_1)\cos(\theta_1) & \dots & \cos(\theta_1)\cos(\theta_N) \\ \vdots & \ddots & \vdots \\ \cos(\theta_N)\cos(\theta_1) & \dots & \cos(\theta_N)\cos(\theta_N) \end{bmatrix} + \begin{bmatrix} \sin(\theta_1)\sin(\theta_1) & \dots & \sin(\theta_1)\sin(\theta_N) \\ \vdots & \ddots & \vdots \\ \sin(\theta_N)\sin(\theta_1) & \dots & \sin(\theta_N)\sin(\theta_N) \end{bmatrix} \tag{3}$$

We define the two vectors, the "cosine" vector $\mathbf{c} = (\cos(\theta_1), \cos(\theta_2), ..., \cos(\theta_N))^T \in \mathbb{R}^N$, and the "sine" vector $\mathbf{s} = (\sin(\theta_1), \sin(\theta_2), ..., \sin(\theta_N))^T \in \mathbb{R}^N$, and rewrite the matrix as $\mathbf{iPL} = \mathbf{cc}^T + \mathbf{ss}^T$.

This matrix is symmetric and has ones on the diagonal, as $\mathbf{iPL}_{ii} = \cos(\theta_i - \theta_i) = \cos(0) = 1$ Its trace is thus $Tr(\mathbf{iPL}) = N$. Importantly, this decomposition demonstrates that the matrix is a rank 2 matrix, which, being symmetric, will only have 2 non null eigenvalues λ_1 and λ_2 and their associated eigenvectors (as observed by (22)). This also implies that, as the sum of the eigenvalues of a matrix is equal to the trace of the matrix, $Tr(\mathbf{iPL}) = N = \lambda_1 + \lambda_2$. Moreover, the two non-trivial eigenvectors will be a linear combination of $\mathbf{c}$ and $\mathbf{s}$, so they will be of the form $A\mathbf{c} + B\mathbf{s}$. Thus, we only need to compute the two scalar values A and B to find the eigenvectors. The eigenvalue equation $\mathbf{iPL}(A\mathbf{c} + B\mathbf{s}) = \lambda(A\mathbf{c} + B\mathbf{s})$ means that:

$$\begin{aligned} \mathbf{iPL}(A\mathbf{c} + B\mathbf{s}) = (\mathbf{cc}^T + \mathbf{ss}^T)(A\mathbf{c} + B\mathbf{s}) = \\ \mathbf{cc}^T A\mathbf{c} + \mathbf{cc}^T B\mathbf{s} + \mathbf{ss}^T A\mathbf{c} + \mathbf{ss}^T B\mathbf{s} = \\ A||\mathbf{c}||^2\mathbf{c} + B\mathbf{c}^T\mathbf{s}\mathbf{c} + A\mathbf{s}^T\mathbf{c}\mathbf{s} + B||\mathbf{s}||^2\mathbf{s} \end{aligned} \tag{4}$$

Let us define the following quantities:

$$\begin{aligned} \gamma &= ||\mathbf{c}||^2 \\ \sigma &= ||\mathbf{s}||^2 \\ \xi &= \mathbf{c}^T\mathbf{s} = \mathbf{s}^T\mathbf{c} \end{aligned} \tag{5}$$

We can then rewrite $\mathbf{iPL}(A\mathbf{c} + B\mathbf{s}) = (A\gamma + B\xi)\mathbf{c} + (A\xi + B\sigma)\mathbf{s}$, which needs to be equal to $\lambda(A\mathbf{c} + B\mathbf{s})$. We therefore have a system of equations:

$$\begin{cases} A\gamma + B\xi = \lambda A \\ A\xi + B\sigma = \lambda B \end{cases} \tag{6}$$

By dividing the two equations we obtain: $\frac{A}{B} = \frac{A\gamma + B\xi}{A\xi + B\sigma}$. Since the eigenvectors remain eigenvectors if they are divided by an arbitrary constant, we impose that $A = 1$. Therefore, we obtain $B^2\xi + B(\gamma - \sigma) - \xi = 0$, so, $\Delta = (\gamma - \sigma)^2 + 4\xi^2$ and:

$$B_{1,2} = \frac{(\gamma - \sigma) \pm \sqrt{(\gamma - \sigma)^2 + 4\xi^2}}{2\xi} = \frac{(\gamma - \sigma) \pm \sqrt{\Delta}}{2\xi} \tag{7}$$

So, the two eigenvectors $\mathbf{v_1}$ and $\mathbf{v_2}$ are:

$$\begin{aligned} \mathbf{v_1} &= \mathbf{c} + B_1\mathbf{s} \\ \mathbf{v_2} &= \mathbf{c} + B_2\mathbf{s} \end{aligned} \tag{8}$$

2.4 Analytical computation of Eigenvalues of iPL Matrix

To compute the eigenvalues we have to show first that $\gamma + B\xi = \sigma + \frac{\xi}{B}$ for both B_1 and B_2. We prove it for B_1, the proof for B_2 is analogous:

$$\begin{aligned}\sigma-\gamma &= \frac{2(\sigma-\gamma)(\sigma-\gamma+\sqrt{\Delta})}{2(\sigma-\gamma+\sqrt{\Delta})} = \frac{-4\xi^2+2(\sigma-\gamma)\sqrt{\Delta}+(\sigma-\gamma)^2+4\xi^2+(\sigma-\gamma)^2}{2(\sigma-\gamma+\sqrt{\Delta})} \\ &= \frac{-4\xi^2+(\sigma-\gamma+\sqrt{\Delta})^2}{2(\sigma-\gamma+\sqrt{\Delta})} = \frac{-2\xi^2}{\sigma-\gamma+\sqrt{\Delta}}+\frac{\sigma-\gamma+\sqrt{\Delta}}{2} = -\frac{\xi}{B_1}+\xi B_1 \\ &\Rightarrow \gamma+B_1\xi = \sigma+\frac{\xi}{B_1}\end{aligned} \tag{9}$$

Using again the eigenvalue equation, we compute the eigenvalue λ_1:

$$(\mathbf{iPL}\cdot\mathbf{v_1})_i = \lambda_1\mathbf{v_1}_i \Rightarrow \lambda_1 = \frac{(\mathbf{iPL}\cdot\mathbf{v_1})_i}{\mathbf{v_1}_i} \tag{10}$$

where

$$\begin{aligned}(\mathbf{iPL}\cdot\mathbf{v_1})_i = \sum \mathbf{iPL}_{ij}\mathbf{v_1}_j = \\ (\cos(\theta_i)\mathbf{c}+\sin(\theta_i)\mathbf{s})^T(\mathbf{c}+B_1\mathbf{s}) = \cos(\theta_i)\gamma+\cos(\theta_i)B_1\xi+\sin(\theta_i)\xi+\sin(\theta_i)B_1\sigma = \\ \cos(\theta_i)(\gamma+B_1\xi)+B_1\sin(\theta_i)(\sigma+\frac{\xi}{B_1}) = \\ (\gamma+B_1\xi)(\cos(\theta_i)+B_1\sin(\theta_i))\end{aligned} \tag{11}$$

So, given that $\mathbf{v_1}_i = \cos(\theta_i)+B_1\sin(\theta_i)$, we have that:

$$\lambda_1 = \frac{(\mathbf{iPL}\cdot\mathbf{v_1})_i}{\mathbf{v_1}_i} = \gamma+B_1\xi = \sigma+\frac{\xi}{B_1} \tag{12}$$

and we obtain λ_2 similarly:

$$\lambda_2 = \frac{(\mathbf{iPL}\cdot\mathbf{v_2})_i}{\mathbf{v_2}_i} = \gamma+B_2\xi = \sigma+\frac{\xi}{B_2} \tag{13}$$

2.5 Two cases of interest

We now look at two limit cases, both of interest for the dynamic analysis of the $\mathbf{iPL}$ matrix.

The first case is $\lambda_1 = N$, which implies $\lambda_2 = 0$. The $\mathbf{iPL}$ matrix then has rank 1, as it only has 1 non null eigenvalue, see Figure 2, panel A. In this case, the $\mathbf{c}$ vector is parallel to the $\mathbf{s}$ vector. A rank 1 matrix with ones on the diagonal must have all elements equal to plus or minus one, i.e., this is the trivial case where all signals are in phase or antiphase: $\overrightarrow{\theta} = (\theta_0+(2k_1+1)\pi, \theta_0+(2k_2+1)\pi, \theta_0+(2k_3+1)\pi, ...\theta_0+(2k_N+1)\pi)^T, k_{1...N}\in\mathbb{Z}$. Then the matrix is maximally rank deficient and contains minimal information. Physiologically, this is the case of maximally phase locked signals, which occurs as the first eigenvalue λ_1 tends to N.

The second case is when $\lambda_1 = \lambda_2 = N/2$, see Figure 2, panel B. Given the constraints on the $\mathbf{iPL}$ matrix, this is possible if and only if $\mathbf{c}$ and $\mathbf{s}$ are orthogonal, their norms are equal and both equal to $N/2$, which is proven as follows. Given that the eigenvalues are $\gamma+B_1\xi$ and $\gamma+B_2\xi$, and $\gamma\neq 0$, by imposing $B_1 = B_2$ we have $\Delta = 0$ and therefore $\xi = 0$ and $\sigma = \gamma$. This means that $\mathbf{c}$ and $\mathbf{s}$ are orthogonal and they have same norm, which is $\gamma = \sigma = N/2 = \lambda_1 = \lambda_2$. Note that if they are orthogonal it means that the two eigenvectors are $\mathbf{c}$ and $\mathbf{s}$ themselves, because $\mathbf{iPLc} = (\mathbf{cc}^T+\mathbf{ss}^T)\mathbf{c} = \mathbf{cc}^T\mathbf{c} = \gamma\mathbf{c}$ and similarly $\mathbf{iPLs} = \sigma\mathbf{s}$.

Therefore, this is the case where the information contained in the $\mathbf{iPL}$ matrix is maximally irreducible to a single eigenvector, and therefore there is no "leading" eigenvector as the connectivity pattern is fully expressed by two orthogonal components which are both equally important, as the relative magnitude of the eigenvalues represents their contribution to the total information contained in the iPL matrix. An example of this configuration is a four blocks matrix where the two diagonal blocks are ones, all signals in phase, and the two non-diagonal blocks are zero, all signals in quadrature, see Figure 2, panel B.

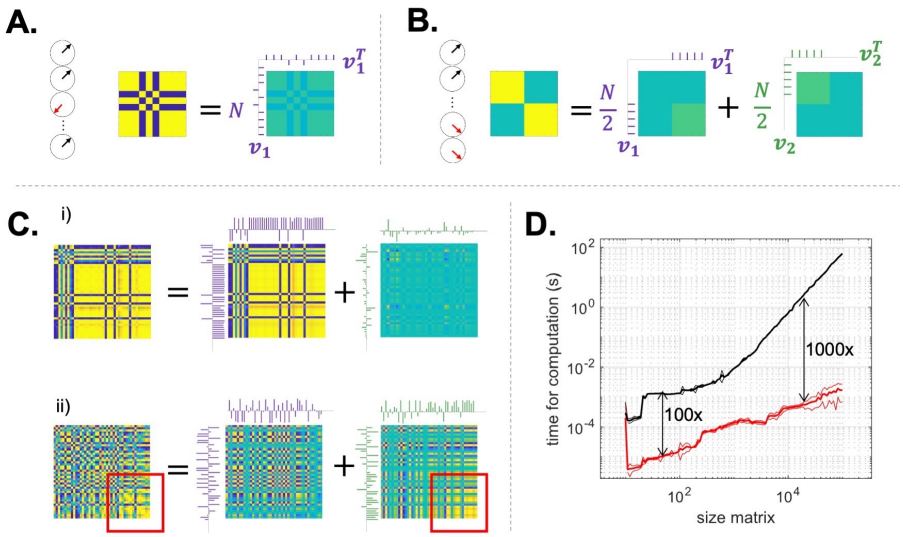

Figure 2: Illustration of the eigenvalue decomposition of limit cases matrices in **A** and **B** corresponding to $\lambda_1 = N$ and $\lambda_1 = \lambda_2$, and instructing exemplars from the rat data in **C**. Purple and green ticks indicate the first and second eigenvectors respectively. **A**. Rank 1 matrix: all signals are either in phase or in anti-phase, as indicated by the clocks. The matrix can be decomposed into a single eigenvector, with maximum eigenvalue $\lambda_1 = N$. **B**. Both eigenvectors are equally important: the first N/2 signals are in quadrature with the second N/2. The two blocks of the matrix are reconstructed by summing 50% of the first eigenvector and 50% of the second. The eigenvalues are both equal to N/2. In this case, discarding one eigenvector would result in losing half of the information contained in the iPL matrix. **C**. Two interesting cases from our data. In the first one (i), the value of the first eigenvector is high, $\lambda_1 = 39$ out of a maximmum of 44, and contains most of the information. It is noticeable that in this case almost all signals are either in phase or in anti-phase, as can be seen from the large blocks. In the second case (ii), $\lambda_1 = 23$, close almost N/2=22. In this case, the two eigenvectors contain almost the same amount of information. Throwing away the second one would lead to a large error in the reconstruction of the matrix: the information on the in phase hub highlighted by the red square is indeed contained in the second eigenvector. **D**. Average speed in seconds (mean, continous line, plus or minus one standard deviation, dotted line) of our algorithm (red line) and the gold standard algorithm for iPL analysis (LEiDA), as a function of the size of the iPL matrix in a log log plot. Black arrows indicate that the black line is 100 or 1000 times the red one.

In view of these considerations, we define, for a specific recording, the Irreducibility Index. The total information in the matrix is the sum of two orthogonal components, the eigenvectors, scaled by the two eigenvalues. If the first eigenvalue is lower than a percentage of $N = \lambda_1 + \lambda_2$, then this means that reducing the $\mathbf{iPL}$ matrix to the first eigenvector would keep less than this percentage of the information. First, we need to define a threshold representing the minimum amount of information one wants to be explained if we used only the first eigenvector, this threshold is expressed as a percentage of N. The Irreducibility Index is then the proportion of time during the recording in which the first eigenvalue of the $\mathbf{iPL}$ matrix is lower than the predefined threshold. If the experimenter requires to keep at least $x\%$ of the information at each time step, the Irreducibility Index at a level $x\%$ indicates the fraction of the recording in which reduction to the first eigenvector would fail in keeping this information. Thus a higher Irreducibility Index reflects a larger negative impact of relying on just the leading eigenvector.

2.6 Two new measures based on iPL eigenvalues

We have found a unique number that characterizes the $\mathbf{iPL}$ matrix, namely, the first eigenvalue λ_1, which is by itself informative on all the N eigenvalues, given that $\lambda_2 = N - \lambda_1$ and all the other eigenvalues are null. This value turns out to be the spectral radius of the $\mathbf{iPL}$ matrix, which, as the matrix is symmetric, corresponds to its 2-norm. So, it is a closed form computable norm of the instantaneous phase locking matrix ((44)). Indeed, we showed that its value, as it gets closer to N, shows that all signals tend to the "trivial" maximal norm situation where they all are in phase or antiphase and, at the same time, the matrix loses information and complexity becoming maximally rank deficient and so maximally ordered. On the other hand, the more it approaches $N/2$, the more the matrix is maximally irreducible to a single connectivity pattern and therefore one sees a less structured phase locking pattern.

Given the considerations above, the first eigenvalue can be considered a global information metric about the instantaneous phase locking of the signals, that is conceptually similar to the Kuramoto Order Parameter ((29; 2; 27; 24; 48; 21; 49; 50)); note that the latter, however, is based on a specific model of the structure of the phase interactions, that is mean phase. Therefore, we define a new measure of metastability, the standard deviation over time of λ_1, which is also equal to the standard deviation of λ_2. We call this measure "Spectral Metastability" as the first eigenvalue is the spectral radius of the **iPL** matrix.

$$\mathbf{meta}_{spec} = \text{std}(\lambda_1) = \text{std}(\lambda_2) \tag{14}$$

2.7 Two new approaches to analyze eigenvector dynamics

The sections above demonstrated that the $N \times N$ **iPL** matrix can be fully and losslessly decomposed into two eigenvectors of size N and one eigenvalue. Based on this, we propose two approaches to analyze the dynamics of eigenvectors and eigenvalues over time. The first one is called "Discrete EiDA", because it finds k discrete states by clustering the eigenvectors and follows the same philosophy as the original LEiDA. The second is called "Continous EiDA" because it interprets the reconfiguration of eigenvectors as a continuous trajectory and quantifies its overall position and speed in a 2-D space. Based on dynamical considerations on the evolution of eigenvectors, as we will do in 3.2, the experimenter can choose to use the first or the second approach.

2.7.1 Discrete EiDA

Discrete EiDA proposes to combine the first and the second eigenvector, normalized and weighted by the square root of their eigenvalues, at a specific time t into a unique $2N$ sized array. It then merges all the arrays coming from the R recordings of a group, having then a set of $R \times T$ arrays. The final step performs k-means clustering using the cosine distance to find k centroids, which are identified as k phase-locking states. The clustering of the first eigenvectors was already proposed in previous approaches ((15; 27; 47; 21; 26; 25)). Here instead we propose to consider both eigenvectors because, as we have seen, the rank 2 **iPL** makes it possible to do clustering of the full information contained in the matrix in a lossless and efficient manner. This is relevant as demonstrated in 3): in the data considered here, discarding the second eigenvector would neglect a significant amount of information, as indicated by the Irreducibility Index.

Having found the clusters, it is then possible to visualize their representative states, the centroids C_i, in a matrix with $C_i^{h1}(C_i^{h1})^T + C_i^{h2}(C_i^{h2})^T$ where C_i^{h1} is the first half of the i^th centroid array and C_i^{h2} is the second half, each corresponding to an eigenvector. We note that using the eigenvectors weighed by the square root of their eigenvalues corresponds to a classic eigendecomposition (EVD) based reconstruction of the matrix. Moreover, given the clusters, it is possible to use the same synthetic measures of the duration of states as defined with LEiDA ((15; 47; 21; 26; 25)), in particular:

1) The Fractional Occurrence of a state, i.e. the relative amount of time in the recording in which the eigenvectors belong to a each cluster.

2) The Dwell Time, i.e. the average duration of a cluster.

These two measures are not equivalent: a state could appear very frequently in a recording, i.e. have a high fractional occurrence, but be on average for a very brief time: have a low dwell time).

2.7.2 Continuous EiDA

It is important to note that, in some recordings, eigenvectors may not be in a discrete set of states so while clusters can always be sought, they might not be meaningful. This may be because k-means may not converge to a robust number of well defined states, or the phase locking space/eigenspace is explored in a homogeneously continuous manner, as we will see below. In this case, the continuous exploration of Phase Locking configurations may be analyzed by plotting the dynamic walk of connectivity motifs in a 2D embedding ((51; 52)).

Therefore, we introduce an approach that examines the evolution of both eigenvectors over time as a continuous flow and call it Continuous EiDA in contrast to the Discrete EiDA described in the previous section.

To do so, we propose following the time evolution of **iPL** in a two dimensional position-speed space, using both eigenvectors in a kinematic speed-displacement (KSD) plot (53) . These two dimensions we consider are: the "position" (overall configuration) $p(t)$, and the "speed" of evolution $s(t)$. The position is what the previous sections have demonstrated to be the best summary indicator of the state of the phase locking matrix: its first eigenvalue (spectral radius). The speed is the "reconfiguration speed" (as already proposed by (31; 27)),at which eigenvectors evolve in

their space, computed as the similarity between temporally adjacent eigenvectors. For an eigenvector **v**, we define its reconfiguration speed $s(t)$ as:

$$s(t) = 1 - |\mathrm{R}(\mathbf{v}(t), \mathbf{v}(t-1))| \tag{15}$$

Where R is the Pearson Correlation Coefficient.

2.8 Existing measures of signal complexity

We compared our metrics with well-known measures of phase locking.

A simple measure of metastability can be obtained from one of the most popular measures of synchronisation: the Kuramoto Order Parameter

$$r = \frac{1}{N}\sum_{i=1}^{N} e^{i\theta_i(t)} \tag{16}$$

that can be computed for each time $\theta_1(t)$, using the phases of the analytical signals((29; 2; 24; 27; 48; 21; 49; 50)). The modulus of $r \in [0, 1]$ is a measure of synchronization: if all signals are in phase, this number approaches 1, while, if they are distributed uniformly, it will approach 0. It can be conceived as a centroid of instantaneous phases. Starting from this number, metastability is defined as its standard deviation over time ((29; 2; 24; 27; 48; 21; 49; 50)), and we refer to it as Kuramoto metastability to clearly differentiate it from the spectral metastability introduced above.

$$\mathbf{meta}_{kop} = \mathrm{std}(|r(t)|) \tag{17}$$

In order to have a proxy for the informational complexity of the evolution of the eigenvectors, we computed the number of bits required to compress it using the lossless data compression Lempel–Ziv–Welch (LZW) algorithm ((54; 55)). A higher complexity, reflected by the need to use more bits to store information, indicates more random and unpredictable patterns as there is more information to store, while a lower one indicates more coherent and structured patterns of evolution with less information to store. Similar approaches have been introduced to quantify perturbational complexity of EEG responses to Transcranial Magnetic Stimulation (TMS) ((56)).

2.9 Application of EiDA to rat fMRI data

We applied the methods described above to a longitudinal dataset of 48 ageing rats ((33; 32), MacNicol et al, in preparation). A cohort of 48 Sprague Dawley rats, Charles River, UK, were monitored across their full 2 years lifespan and scanned in up to 4 scanning sessions with a 9.4 T Bruker Biospec MR scanner, specifically at the ages of 3, 5, 11 and 17 months. The ages of 3,5,11,17 represent, in general, late adolescence, young adulthood, middle age, and the beginning of senescence ((57)). Experiments were performed in accordance with the Home Office (Animals Scientific Procedures Act, UK, 1986) and approved by King's College London's ethical committee. Resting-state functional data were recorded using a 2D multi-slice multi-echo echo planar imaging sequence with TR = 2750 ms, TEs = 11, 19, 27, and 35 ms, and a 70^o flip angle, producing an image with 40 slices. Slices were 0.5 mm thick with a 0.2 mm gap, which gave a 48×44 matrix, with an in-plane resolution of 0.5 x 0.5 mm. Rats were anesthetized with 1.8% isoflurane for the duration of functional scans. This dose produced anatomically-plausible components from single-subject and group-level Independent Component Analysis (ICA) ((58).

Motion-correction was estimated on the first echo time to its middle volume, and applied identically to each echo time volume. The corrected echo volumes were optimally combined, which maximises the signal-to-noise ratio at the expense of some loss of time resolution ((59)). Signals were simultaneously filtered with a 0.01-0.08 Hz bandpass filter and regressed for nuisance factors, including motion and CSF signal. Corrected and filtered fMRI volumes were warped to a study-specific template ((32))generated and parcellated into 44 anatomical regions of interest (ROI), 22 for each hemisphere, generated by combining delineations of predominantly gray matter structures from two popular rat atlases ((60; 61)). The BOLD signals were averaged within each ROI.

2.10 Statistical Analysis

We only included in our analyses the rats that had survived to the last time-point, which were 30 out of 48 rats. As measures were not normally distributed, we first tested the variation across age groups of all the parameters considered using a non-parametric one way ANOVA test (Kruskal-Wallis test). A post-hoc Wilcoxon rank sum test was then used to test the variability between two different age groups. The multiple comparison correction was performed by controlling the False Discovery Rate (FDR) at a rate $\alpha = 0.05$, using the Benjamini Hochberg procedure.

A Pearson Correlation Coefficient R was used to test collinearity between measures where the test for significance was obtained by calculating an empirical null R distribution by shuffling data.

3 Results

3.1 Static Functional Connectivity

The average connectivity matrices (see Figure 3) show a loss of total correlation and a diminution of the number of correlated areas over the time-span. In Figure 3 we show the evolution of sum of squared values of the connectivity matrices for each rat where the mean sharply decreases from 19.7 ± 3.8 at month 3 to 13.7 ± 3.12 at month 17 with an overall ANOVA significance of e-08 (see Figure 3).

We also computed the average $\mathbf{iPL}$ matrices throughout the recording and computed the sum of squared values for each subject, showing that it follows a similar decrease that is statistically significant (ANOVA e-08). Correlation between the sum of squared values in Pearson matrices and the average $\mathbf{iPL}$ matrices is both significantly, $p<0.001$, and high: $R=0.97$. Figure 3) shows both the Pearson Correlation averaged matrices and the averages of the Instantaneous Phase Locking Matrices and their pairwise correlations.

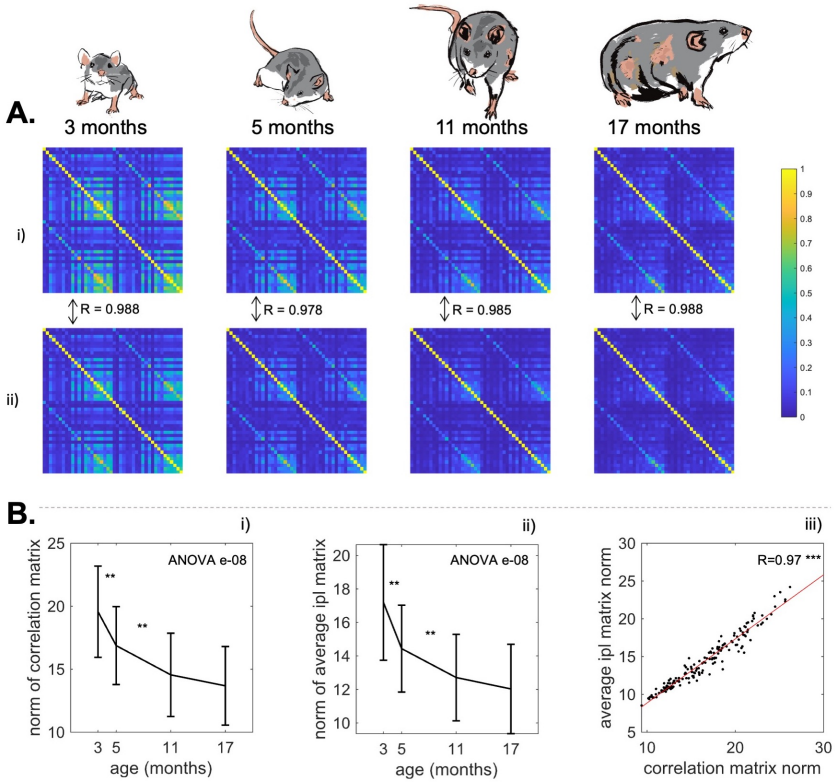

Figure 3: Results from the static analysis **A**. The group averaged Pearson connectivity matrix (i) and time averaged iPL matrix (ii) in the four age groups We indicate the elementwise correlations between the Pearson correlation matrices and the iPL matrices. Ageing is associated with an overall decrease of connected hubs (yellow hubs). **B**. The evolution with ageing (mean +- standard deviation) of the norm of the Pearson correlation matrices (i) and the norm of the averaged iPL matrices (ii). Both the measure show a decrease which quantifies the loss of connectivity strength that is observable in panel A. (iii): Correlation between the two measures with the best Ordinary Least Squares fit. The two measures are highly correlated, meaning that the average iPL matrix conveys the same information as the Pearson correlation matrix and therefore suggests that it may be worth to study its evolution over time. * indicates p<0.05 ** p<0.01 and *** p<0.001.

3.2 Dynamic Functional Connectivity measures: Discrete EiDA

We repeated k-means clustering for k going from 1 to 10 and found that the best number of clusters was $k = 3$ by application of the "elbow rule" (see Supplementary Material): we plotted the sum of squared distances of each data point in a cluster with their centroids as a function of k. The point where this curve presents an elbow (in our case $k = 3$) is often chosen as the optimal number of clusters, because it indicates that adding another cluster ($k = k + 1$) would not significantly improve the clustering performance. As shown in Figure 4 A, the three centroids are consistent throughout the four age groups. however, the first two centroids, which are related to phase-locked hubs, show a significant (ANOVA e-06) decrease of dwelling time, while the third, which is related to non-connected and more random patterns, shows an increase both in dwell time and fractional occurrence, Figure 4 B.

Two pieces of evidence suggest that in these data Continous EiDA is preferable to its Discrete counterpart. The first is that the centroids 1 and 2 are very similar, which means that they may result from the erroneous partitioning of a single cluster. The second is that the third cluster, due to its very low overall values, could represent a noise component rather than an actual brain state. This is also coherent with its increase in fractional duration with ageing. Silhouette Coefficient Analysis (see Supplementary Material) seems to confirm that clusters are not well-defined in our data.

For the reasons above, we will consider Continuous EIDA as the primary outcome of our study.

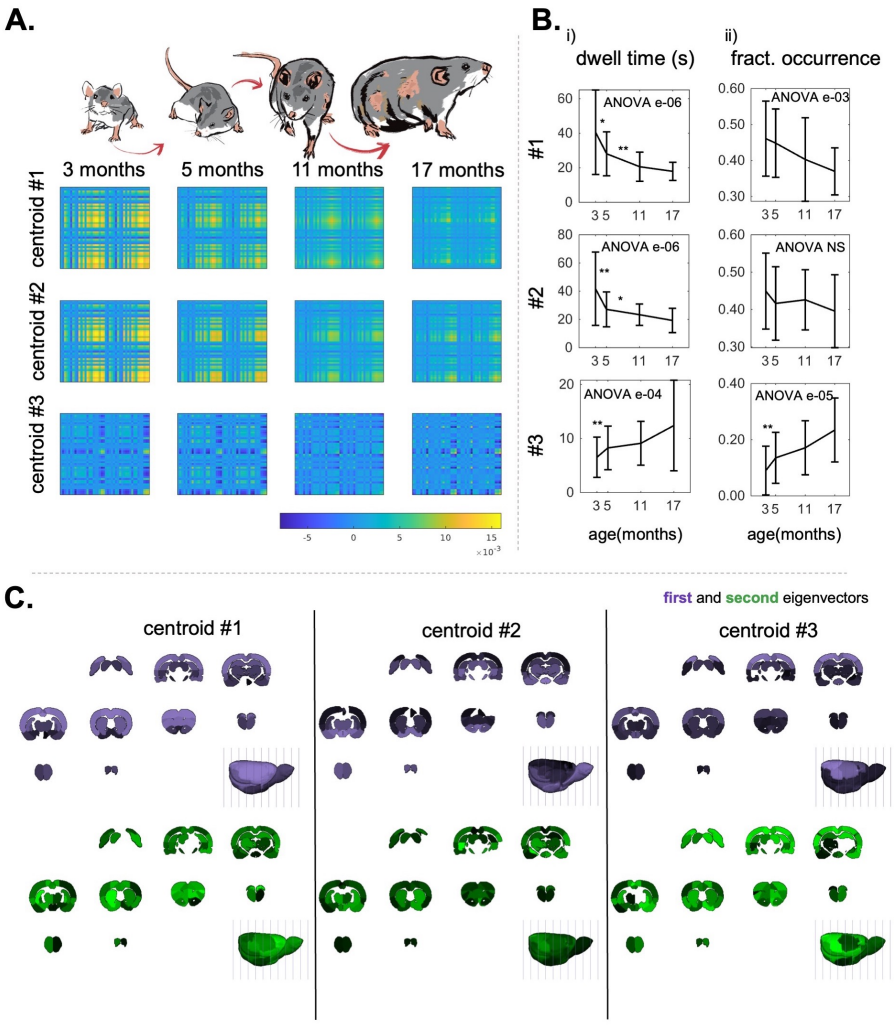

Figure 4: Results for the Discrete EiDA **A**: The three EiDA cluster centroids and their evolution with ageing. Each row represents a centroid, each column a different age group **B**: the evolution with ageing of (i) dwelling time and (ii) fractional occurrence of clusters. The first two clusters, that are associated with connected hubs and reflect the connectivity information contained in the Pearson correlation matrices, become less frequent in the recordings as rats age. On the other hand, the third cluster, which is associated with a less structured and weaker connectivity pattern, increases in both dwell time and fractional occurrence with ageing. * indicates $p<0.05$ ** $p<0.01$ and *** $p<0.001$. **C**. The cluster centroids represented in anatomical space, with the first eigenvector in purple and the second eigenvector in green. The real connectivity pattern would be the sum of the connectivity patterns expressed by the two eigenvectors. We show here the centroids for the three clusters in the 3 months age group.

3.3 Dynamic Functional Connectivity measures: Continuous EiDA

The position and speed plots over the recording of a representative rat are shown in Figure 5 A. We found that the trajectories change with ageing. Patterns started as trajectories with a broad exploration of the configuration space and finished confined to a more compact area. Moreover, as measured below, the trajectories of younger rats exhibit a higher contribution from the first-eigenvector.

Figure 5 B shows in the same representative rat, the transformation from the raw data to the eigenvector evolution using EiDA, in a specific portion of the recording, both for 3 months and 17 months. In the first case signals are highly phase locked, as observable in the data. This is indicated by a more compact and ordered evolution of the eigenvectors. On the other hand, in the 17 months case, where there is almost no phase locking, eigenvectors evolve in a less compact and structured manner. Informational complexity, as explained below, will quantify this result.

As shown in Figure 5 C.i, the average of the first eigenvalues per recording show a statistically significant decay with ageing (from 29.5 $\pm$ 1.8 to 27.0 $\pm$ 1.0, ANOVA e-08). As in the case of static connectivity, this decay plateaued from 11 months to 17 months, suggesting that there is no significant change from middle-age to senescence. We observed a significant (ANOVA p= e-05) increase of reconfiguration speed of the first eigenvector with ageing, and a non-significant increase in speed of the second eigenvector from 3 months to 11 months (Figure 5 C.ii). Hence ageing is associated with an overall loss of structure in the "walk" of the connectivity configurations (this is also shown by the increase of the informational complexity in Figure 5 C.iv, see below), and the correlation between adjacent eigenvectors diminishes and consequently the reconfiguration speed, defined as 1-correlation of adjacent eigenvectors, increases. On the other hand, the second eigenvector, representing the less structured component, does not exhibit a significant increase of reconfiguration speed. The two speeds show an overall positive correlation of 0.62, p<0.001, as shown in Figure 5 D.ii.

We observed an increase (ANOVA e-08) in the Informational Complexity measure defined in 2.8with ageing. This age-dependent increase of informational complexity indicates that connectivity configurations evolve in a more random and less structured way in older rats compared with younger rats, as in Figure 5, B. We correlated informational complexity with the average value of the leading eigenvalue per recording, obtaining an overall correlation of -0.95, p<0.001 Fig 5 D.i .It is interesting to note that this strongly negative correlation (R=-0.95, p<0.001) establishes an information theoretical relation between the first eigenvalue and the amount of information contained in the $\mathbf{iPL}$ matrix, as also explained in 2.5.

Figure 5 C.iii shows the Irreducibility Index with four thresholds of 70, 65, 60 and 55%. The Irreducibility Index with a threshold of 65% is greater than 0.4 in 3 months rats and becomes greater than 0.7 in 17 months rats. This means that discarding the second eigenvector would neglect a significant (more than 35%) amount of functional connectivity information over the life-span of the rats. Same considerations hold for the Irreducibility Index with thresholds of 60 and 70 %. Interestingly, for thresholds between 60 and 70%, information loss increases with age.

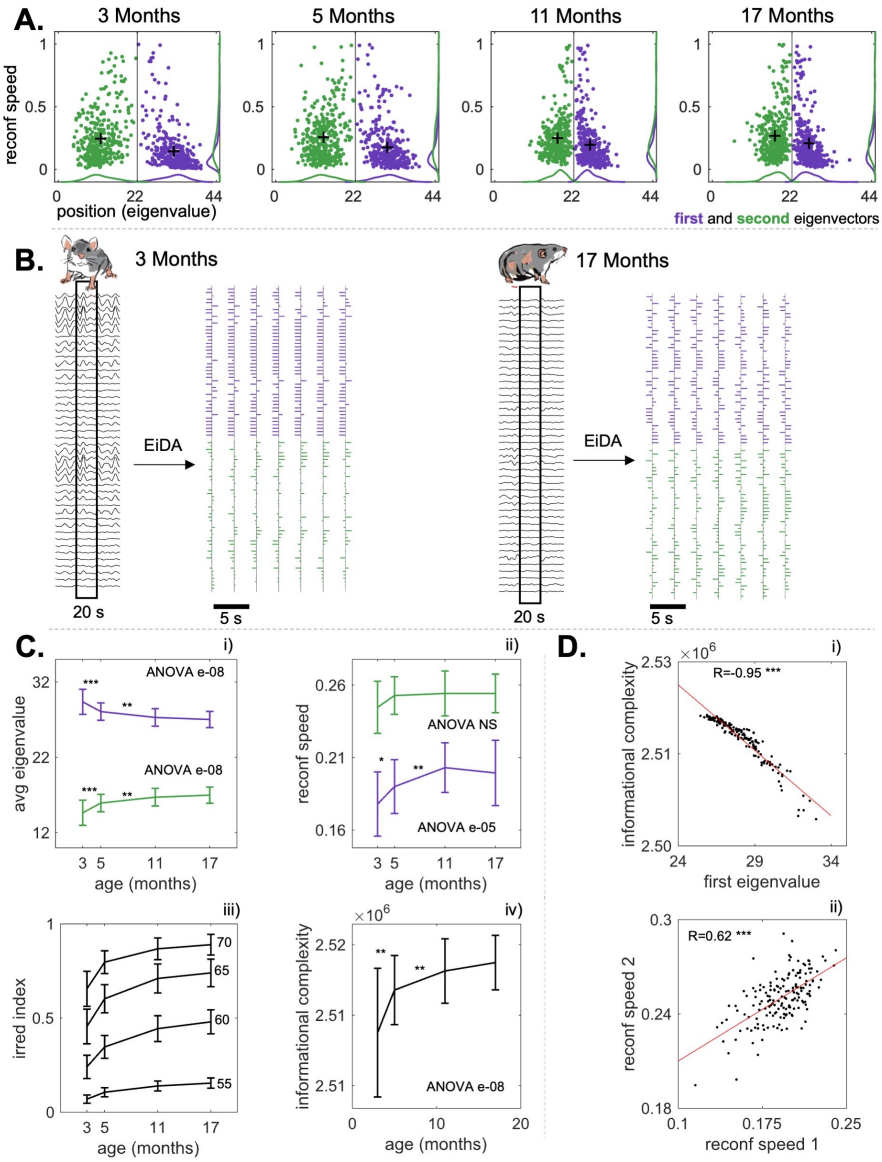

Figure 5: Results for the Continuous EiDA **A**. The position-speed evolution of a representative rat. Crosses represent the centers of mass of the distributions. Patterns evolve from a broader exploration of the space to a more compact one with age, where the leading eigenvalues decreases on average and reconfiguration speeds grow. This means that connectivity patterns over time start from a more structured regime (less speed, higher eigenvalues) to a more random one. **B**. The raw data and the evolution of the two eigenvectors in two different cases: 3 months (left) and 17 months (right). Note that in the first case there is more instantaneous connectivity, as can be seen from the raw data. This is related to a more ordered and compact evolution of eigenvectors, and the fact that the first eigenvector contains most of the information. In the second case there is almost no instantaneous connectivity, as shown by the static results in Fig 3. This is reflected by more random, less compact and equally informative eigenvectors **C**. the measures of interest: (i) average eigenvalue per recording (mean $\pm$ variance, first eigenvalue in purple, second in green). The first eigenvalue shows a decrease over time, in line with the loss of structure that is noticeable in panel B. (ii) average reconfiguration speed of first (purple) and second (green) eigenvector, which reflects the fact that eigenvectors evolve faster with ageing (iii) Irreducibility Index, we plot 4 thresholds: 70, 65, 60, 55% (iv) informational complexity of the time course of eigenvalues. Plot (iii) has no significance indicated because we are not interested in the effect of ageing but on the fact that a non negligible amount of the recordings is not irreducible to a single eigenvector. Moreover, for visual clarity, in plot (iii) mean $\pm$ half of the variance is showed. **D**. (i) Correlation between informational complexity and first eigenvalue, which is larger than 0.9. reflecting that the higher the first eigenvalue is, the lower the amount of information contained in the iPL matrix is. (ii) correlation between the reconfiguration speed of the two eigenvectors. * indicates p<0.05 ** p<0.01 and *** p<0.001.

From the KSD plots in Figure 5, we observe that as the rats age, there is a reduced exploration of the position-speed space. We quantify the quality of the exploration with the standard deviation of the first eigenvalue over the recording, the spectral metastability. We found that spectral metastability declines with age (ANOVA e-06) (Figure 6). This new measure of metastability and the Kuramoto metastability are related: through a quadratic fit we found that the relation between spectral metastability and the Kuramoto metastability is the following: $y = 0.004x^2 - 0.012x + 0.013$, adjusted R squared = 0.59 (Figure 6). We used the MATLAB R2022b function *polyfit*.

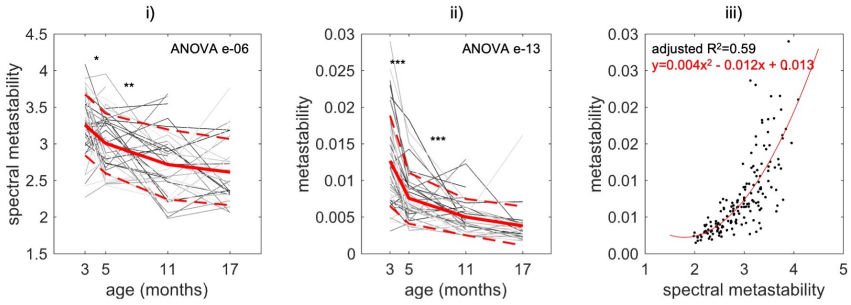

Figure 6: The evolution with ageing of (i) metastability and (ii) spectral metastability. Red lines indicate means, dotted lines indicate standard deviations. Here, the individual trajectories (gray lines) of each single rat are showed. Some lines present discontinuities in case the recording for a specific rat and age group was missing. Ageing is associated with a significant decrease of both metastability and our proposed measure of spectral metastability (iii) Scatter plot of spectral metastability versus metastability. The red line represents the quadratic fit that was performed to explain metastability as a function of spectral metastability. * indicates p<0.05 ** p<0.01 and *** p<0.001.

3.4 Computation Times

We measured the time necessary to compute the EVD of the $\mathbf{iPL}$ matrix and compared our approach with the benchmark algorithm for LEiDA, implemented in Matlab, by varying the matrix size logarithmically from $N = 10$ to $N = 10^5$ and generating 20 $\mathbf{iPL}$ matrices for each size. As shown in Figure 2 D, with our computer (Intel(R) Xeon(R) Silver 4116 CPU @ 2.10GHz), EiDA is 100 times faster for matrices with dimensions of 100x100, and becomes 1000 times faster for matrices larger than 10,000x10,000. Note that the matrix decomposition in the two eigenvectors also allows to save each matrix with $2N$ elements instead of $\frac{N(N-1)}{2}$. Computational speed should ease the extension of EiDA to higher dimensionality both in space and time.

4 Discussion

In this study we set out to explore the implications of using LEiDA for dimensionality reduction in dFC studies, to investigate reconfiguration dynamics in addition to state dynamics, and to test our novel adaptated method to resting-state fMRI data from an ageing rat study. Our resulting method, EiDA, provides an analytically principled framework for dimensionality reduction and dynamical analysis, and demonstrates utility from a number of theoretical and application perspectives.

4.1 Eigenvector decomposition of the iPL matrix

EiDA provides an analytical solution expressible in closed form for the lossless decomposition of the instantaneous Phase Locking matrix. Complete information is encoded in two eigenvectors and one eigenvalue, allowing the calculation of conventional dynamic metrics and the derivation of novel measures to further characterize the dynamic evolution of the spontaneous activity in the resting-state brain.

4.2 First eigenvalue in Hilbert transformed time-series

As EiDA is an eigenvector decomposition of the $\mathbf{iPL}$ matrix, one could be tempted to interpret the eigenspace spanned by first eigenvector as the denoised form of the matrix. However this may not be necessarily true as there is no clear differentiation of signal and noise, particularly in the regime where λ_1 is far from N. One could articulate an interpretation of the leading eigenvector as the container of the large scale information about the connectivity patterns, while the second eigenvector contains more localized details, following ideas from graph signal analysis (62). However,

this interpretation breaks down in the regime where $\lambda_1 \approx \lambda_2$ as shown by the counter example of Figure 2, where in a fully structured matrix, made of 4 blocks, the two eigenvalues are equal, and using only the first eigenvector would discard 50% of the overall phase locking information. In conclusion, it is necessary to consider both eigenvectors.

The analytical derivation in this paper allows the rigorous definition of a global parameter, the first eigenvalue of the $\mathbf{iPL}$ matrix, whose distribution over time contains the information on global connectivity; the standard deviation of this distribution we have defined as a novel estimator of metastability.

This eigenvalue can be a more accurate indicator than the Kuramoto Order Parameter of the phase locking structure, being the 2-norm of the phase locking matrix, rather than the centroid of instantaneous angles. For example, in a maximally synchronized and ordered state, as in Figure 2, where all the signals are either in phase or in antiphase, the Kuramoto Order Parameter can be 0 if half of the signals are in phase and the other half in antiphase, whilst the first eigenvector would reach its maximal possible value and capture the "singular" structure of this configuration.

The methodology can be used to extract discrete states whenever the time-series of the two eigenvectors would warrant the use of clustering; and in addition, continuous EiDA can provide a complementary perspective to discrete states by capturing the evolution of the dynamics in 2-dimensional plots. Metrics from both discrete and continuous EiDA may provide more accurate estimations of differences between case and control groups, and so may improve discrimination and classification accuracy of putative neuromechanistic biomarkers (24).

Finally, the analytical methods significantly accelerate the calculation of the orthogonal decomposition and enable its extension to much higher dimensional data, either or both in space and time.

4.3 Dynamical and complexity insights for ageing

Static results show a decrease of connectivity through ageing that is reflected and refined by the dynamical analysis, grounding the results obtained with the dynamic approach.

Results on the brain dynamics were obtained using the continuous version of EiDA as there was limited evidence from the data to support discrete brain states. EiDA was able to capture the changes of the spatiotemporal patterns of connectivity that clearly showed a loss of phase synchrony and a reduced connectivity structure with ageing. This in line with previous results obtained with other methodologies both in static and dynamic functional connectivity studies of ageing ((38; 34; 40; 41; 31; 63)).

Retaining just the leading eigenvector as in LEiDA, appears to result in an age-related increase in dFC information loss. This implies, that in ageing, more information is contained in the 2nd eigenvector. This is interesting as one can interpret the 2nd eigenvector as reflecting more localized connectivity information (62). This is in agreement with previous studies (64; 65) where healthy ageing was associated with a shift in local/global balance, with less information coded in global interactions and more in in local dynamics.

The increase of the reconfiguration speed of the first eigenvector associated with ageing is also interesting as the brain dynamics are shown to move from a relatively coherent exploration of the kinematic space to a more random exploration with ageing, as pointed out by (37). Increases in complexity with healthy ageing have previously been found using point-wise correlation dimension (66) and multi-scale entropy (64; 65) in resting-state neuroimaging which is congruent with our findings. Taken together, this picture is particularly compelling as it is found using two methods grounded in different theories: dynamical system analysis and information theory. Furthermore, by using our analytical interpretation and by correlating eigenvalues with informational complexity, we have established a link between dynamic connectivity analysis and the notion of informational complexity of signals. Finally, a decrease in spectral metastability was observed with ageing, which is in line with previous findings of a proxy measure of metastability based on spatial diversity ((63)).

4.4 Conclusion

EiDA provides a computationally fast, analytically principled, closed form method to extract connectivity information in a lossless manner from signals in high-dimensional time-series. Its application to fMRI data from a longitudinal rat ageing study demonstrated its advantages over conventional methods and revealed a strong relationship between dynamical and informational metrics. This approach holds promise for improving the accuracy of putative neuromechanistic biomarkers of disease or the effects of intervention studies, but also holds potential for applications outside of neuroscience.

The code for EiDA will be available at www.github.com/alteriis on acceptance of this paper for publication.

References

[1] F. E. Turkheimer, F. E. Rosas, O. Dipasquale, D. Martins, E. D. Fagerholm, P. Expert, F. Váša, L. D. Lord, R. Leech, A complex systems perspective on neuroimaging studies of behavior and its disorders, The Neuroscientist : a review journal bringing neurobiology, neurology and psychiatry 28 (2022) 382–399. doi:10.1177/1073858421994784.
URL https://pubmed.ncbi.nlm.nih.gov/33593120/

[2] F. Hancock, F. E. Rosas, P. A. Mediano, A. I. Luppi, J. Cabral, O. Dipasquale, F. E. Turkheimer, May the 4c's be with you: an overview of complexity-inspired frameworks for analysing resting-state neuroimaging data, Journal of the Royal Society Interface 19 (191) (2022) 20220214.

[3] J. Ladyman, J. Lambert, K. Wiesner, What is a complex system?, European Journal for Philosophy of Science 3 (2013). doi:10.1007/s13194-012-0056-8.

[4] K. J. Friston, Transients, metastability, and neuronal dynamics, NeuroImage 5 (1997) 164–171. doi:10.1006/NIMG.1997.0259.

[5] E. D'Angelo, V. Jirsa, The quest for multiscale brain modeling, Trends in Neurosciences 45 (2022) 777–790. doi:10.1016/J.TINS.2022.06.007.

[6] R. M. Hutchison, T. Womelsdorf, E. A. Allen, P. A. Bandettini, V. D. Calhoun, M. Corbetta, S. D. Penna, J. H. Duyn, G. H. Glover, J. Gonzalez-Castillo, D. A. Handwerker, S. Keilholz, V. Kiviniemi, D. A. Leopold, F. de Pasquale, O. Sporns, M. Walter, C. Chang, Dynamic functional connectivity: Promise, issues, and interpretations, NeuroImage 80 (2013). doi:10.1016/j.neuroimage.2013.05.079.

[7] J. R. Cohen, The behavioral and cognitive relevance of time-varying, dynamic changes in functional connectivity (2018). doi:10.1016/j.neuroimage.2017.09.036.

[8] A. A. Fingelkurts, A. A. Fingelkurts, S. Kähkönen, Functional connectivity in the brain - is it an elusive concept?, Neuroscience and Biobehavioral Reviews 28 (2005). doi:10.1016/j.neubiorev.2004.10.009.

[9] K. J. Friston, Functional and effective connectivity: A review, Brain Connectivity 1 (2011) 13–36. doi:10.1089/BRAIN.2011.0008/ASSET/IMAGES/LARGE/FIGURE10.JPEG.
URL https://www.liebertpub.com/doi/10.1089/brain.2011.0008

[10] K. E. Stephan, K. J. Friston, Functional connectivity, Encyclopedia of Neuroscience (2009) 391–397doi:10.1016/B978-008045046-9.00308-9.

[11] E. C. Hansen, D. Battaglia, A. Spiegler, G. Deco, V. K. Jirsa, Functional connectivity dynamics: Modeling the switching behavior of the resting state, NeuroImage 105 (2015). doi:10.1016/j.neuroimage.2014.11.001.

[12] V. D. Calhoun, R. Miller, G. Pearlson, T. Adali, The chronnectome: Time-varying connectivity networks as the next frontier in fmri data discovery, Neuron 84 (2014) 262–274. doi:10.1016/J.NEURON.2014.10.015.

[13] L. M. Arbabyazd, D. Lombardo, O. Blin, M. Didic, D. Battaglia, V. Jirsa, Dynamic functional connectivity as a complex random walk: Definitions and the dfcwalk toolbox, MethodsX 7 (1 2020). doi:10.1016/J.MEX.2020.101168.
URL https://pubmed.ncbi.nlm.nih.gov/33344179/

[14] R. Hindriks, M. H. Adhikari, Y. Murayama, M. Ganzetti, D. Mantini, N. K. Logothetis, G. Deco, Can sliding-window correlations reveal dynamic functional connectivity in resting-state fmri?, NeuroImage 127 (2016). doi:10.1016/j.neuroimage.2015.11.055.

[15] J. Cabral, D. Vidaurre, P. Marques, R. Magalhães, P. S. Moreira, J. M. Soares, G. Deco, N. Sousa, M. L. Kringelbach, Cognitive performance in healthy older adults relates to spontaneous switching between states of functional connectivity during rest, Scientific Reports 7 (2017). doi:10.1038/s41598-017-05425-7.

[16] D. Gabor, Theory of communication. part 1: The analysis of information, Journal of the Institution of Electrical Engineers - Part III: Radio and Communication Engineering 93 (1946) 429–441. doi:10.1049/JI-3-2.1946.0074.

[17] M. L. V. Quyen, J. Foucher, J. P. Lachaux, E. Rodriguez, A. Lutz, J. Martinerie, F. J. Varela, Comparison of hilbert transform and wavelet methods for the analysis of neuronal synchrony, Journal of Neuroscience Methods 111 (2001) 83–98. doi:10.1016/S0165-0270(01)00372-7.

[18] H. Honari, A. S. Choe, M. A. Lindquist, Evaluating phase synchronization methods in fmri: A comparison study and new approaches, NeuroImage 228 (2021). doi:10.1016/j.neuroimage.2020.117704.

[19] E. A. Allen, E. Damaraju, S. M. Plis, E. B. Erhardt, T. Eichele, V. D. Calhoun, Tracking whole-brain connectivity dynamics in the resting state, Cerebral Cortex 24 (2014) 663–676. doi:10.1093/CERCOR/BHS352.
URL https://academic.oup.com/cercor/article/24/3/663/394348

[20] G. Deco, J. Cruzat, J. Cabral, E. Tagliazucchi, H. Laufs, N. K. Logothetis, M. L. Kringelbach, Awakening: Predicting external stimulation to force transitions between different brain states, Proceedings of the National Academy of Sciences of the United States of America 116 (2019). doi:10.1073/pnas.1905534116.

[21] L. D. Lord, P. Expert, S. Atasoy, L. Roseman, K. Rapuano, R. Lambiotte, D. J. Nutt, G. Deco, R. L. Carhart-Harris, M. L. Kringelbach, J. Cabral, Dynamical exploration of the repertoire of brain networks at rest is modulated by psilocybin, NeuroImage 199 (2019). doi:10.1016/j.neuroimage.2019.05.060.

[22] A. S. Olsen, A. Lykkebo-Valløe, B. Ozenne, M. K. Madsen, D. S. Stenbæk, S. Armand, M. Mørup, M. Ganz, G. M. Knudsen, P. M. Fisher, Psilocybin modulation of time-varying functional connectivity is associated with plasma psilocin and subjective effects, NeuroImage 264 (2022) 119716. doi:10.1016/J.NEUROIMAGE.2022.119716.
URL https://linkinghub.elsevier.com/retrieve/pii/S1053811922008370

[23] L. G. S. França, J. Ciarrusta, O. Gale-Grant, S. Fenn-Moltu, S. Fitzgibbon, A. Chew, S. Falconer, R. Dimitrova, L. Cordero-Grande, A. N. Price, E. Hughes, J. O'Muircheartaigh, E. Duff, J. J. Tuulari, G. Deco, S. J. Counsell, J. V. Hajnal, C. Nosarti, T. Arichi, A. D. Edwards, G. McAlonan, D. Batalle, Neonatal brain dynamic functional connectivity: impact of preterm birth and association with early childhood neurodevelopment, bioRxiv (2022) 2022.11.16.516610doi:10.1101/2022.11.16.516610.
URL https://www.biorxiv.org/content/10.1101/2022.11.16.516610v2https://www.biorxiv.org/content/10.1101/2022.11.16.516610v2.abstract

[24] F. Hancock, F. E. Rosas, R. A. McCutcheon, J. Cabral, O. Dipasquale, F. E. Turkheimer, Metastability as a neuromechanistic biomarker of schizophrenia pathology, medRxiv (2022) 2022.10.14.22281093doi:10.1101/2022.10.14.22281093.
URL https://www.medrxiv.org/content/10.1101/2022.10.14.22281093v1https://www.medrxiv.org/content/10.1101/2022.10.14.22281093v1.abstract

[25] C. A. Figueroa, J. Cabral, R. J. Mocking, K. M. Rapuano, T. J. van Hartevelt, G. Deco, P. Expert, A. H. Schene, M. L. Kringelbach, H. G. Ruhé, Altered ability to access a clinically relevant control network in patients remitted from major depressive disorder, Human Brain Mapping 40 (2019) 2771–2786. doi:10.1002/HBM.24559.
URL https://onlinelibrary.wiley.com/doi/full/10.1002/hbm.24559https://onlinelibrary.wiley.com/doi/abs/10.1002/hbm.24559https://onlinelibrary.wiley.com/doi/10.1002/hbm.24559

[26] S. A. Martínez, G. Deco, G. J. T. Horst, J. Cabral, The dynamics of functional brain networks associated with depressive symptoms in a nonclinical sample, Frontiers in Neural Circuits 14 (2020) 60. doi:10.3389/FNCIR.2020.570583/BIBTEX.

[27] F. Hancock, J. Cabral, A. I. Luppi, F. E. Rosas, P. A. Mediano, O. Dipasquale, F. E. Turkheimer, Metastability, fractal scaling, and synergistic information processing: What phase relationships reveal about intrinsic brain activity, NeuroImage 259 (2022). doi:10.1016/j.neuroimage.2022.119433.

[28] F. Cavanna, M. G. Vilas, M. Palmucci, E. Tagliazucchi, Dynamic functional connectivity and brain metastability during altered states of consciousness, NeuroImage 180 (2018) 383–395. doi:10.1016/J.NEUROIMAGE.2017.09.065.

[29] G. Deco, M. L. Kringelbach, V. K. Jirsa, P. Ritter, The dynamics of resting fluctuations in the brain: Metastability and its dynamical cortical core, Scientific Reports 7 (2017). doi:10.1038/s41598-017-03073-5.

[30] L.-D. Lord, Integration and segregation in whole-brain networks: implications for altered states of consciousness, PhD thesis, University of Oxford (2018).
URL /paper/Integration-and-segregation-in-whole-brain-for-of-Lord/bded06176e0702b889b439d56ebdc0d1b8b83392

[31] D. Battaglia, T. Boudou, E. C. Hansen, D. Lombardo, S. Chettouf, A. Daffertshofer, A. R. McIntosh, J. Zimmermann, P. Ritter, V. Jirsa, Dynamic functional connectivity between order and randomness and its evolution across the human adult lifespan, NeuroImage 222 (2020). doi:10.1016/j.neuroimage.2020.117156.

[32] E. MacNicol, P. Wright, E. Kim, I. Brusini, O. Esteban, C. Simmons, F. E. Turkheimer, D. Cash, Age-specific adult rat brain mri templates and tissue probability maps, Frontiers in Neuroinformatics 15 (2022). doi:10.3389/fninf.2021.669049.

[33] I. Brusini, E. MacNicol, E. Kim, Örjan Smedby, C. Wang, E. Westman, M. Veronese, F. Turkheimer, D. Cash, Mri-derived brain age as a biomarker of ageing in rats: validation using a healthy lifestyle intervention, Neurobiology of Aging 109 (2022). doi:10.1016/j.neurobiolaging.2021.10.004.

[34] R. F. Betzel, L. Byrge, Y. He, J. Goñi, X. N. Zuo, O. Sporns, Changes in structural and functional connectivity among resting-state networks across the human lifespan, NeuroImage 102 (2014) 345–357. doi:10.1016/J.NEUROIMAGE.2014.07.067.

[35] Y. Chen, W. Wang, X. Zhao, M. Sha, Y. Liu, X. Zhang, J. Ma, H. Ni, D. Ming, Age-related decline in the variation of dynamic functional connectivity: A resting state analysis, Frontiers in Aging Neuroscience 9 (2017). doi:10.3389/fnagi.2017.00203.

[36] E. N. Davison, B. O. Turner, K. J. Schlesinger, M. B. Miller, S. T. Grafton, D. S. Bassett, J. M. Carlson, Individual differences in dynamic functional brain connectivity across the human lifespan, PLoS Computational Biology 12 (11 2016). doi:10.1371/JOURNAL.PCBI.1005178.
URL /pmc/articles/PMC5120784//pmc/articles/PMC5120784/?report=abstracthttps://www.ncbi.nlm.nih.gov/pmc/articles/PMC5120784/

[37] S. Nobukawa, M. Kikuchi, T. Takahashi, Changes in functional connectivity dynamics with aging: A dynamical phase synchronization approach, NeuroImage 188 (2019) 357–368. doi:10.1016/J.NEUROIMAGE.2018.12.008.

[38] D. H. Salat, The declining infrastructure of the aging brain, https://home.liebertpub.com/brain 1 (2011) 279–293. doi:10.1089/BRAIN.2011.0056.
URL https://www.liebertpub.com/doi/10.1089/brain.2011.0056

[39] K. J. Schlesinger, B. O. Turner, B. A. Lopez, M. B. Miller, J. M. Carlson, Age-dependent changes in task-based modular organization of the human brain, NeuroImage 146 (2017). doi:10.1016/j.neuroimage.2016.09.001.

[40] J. Zimmermann, P. Ritter, K. Shen, S. Rothmeier, M. Schirner, A. R. McIntosh, Structural architecture supports functional organization in the human aging brain at a regionwise and network level, Human Brain Mapping 37 (2016). doi:10.1002/hbm.23200.

[41] J. R. Andrews-Hanna, A. Z. Snyder, J. L. Vincent, C. Lustig, D. Head, M. E. Raichle, R. L. Buckner, Disruption of large-scale brain systems in advanced aging, Neuron 56 (2007) 924–935. doi:10.1016/J.NEURON.2007.10.038.

[42] K. J. Friston, C. D. Frith, P. F. Liddle, R. S. Frackowiak, Functional connectivity: The principal-component analysis of large (pet) data sets, Journal of Cerebral Blood Flow and Metabolism 13 (1993). doi:10.1038/jcbfm.1993.4.

[43] K. J. Friston, Functional and effective connectivity in neuroimaging: A synthesis, Human Brain Mapping 2 (1994). doi:10.1002/hbm.460020107.

[44] J. W. Demmel, Applied Numerical Linear Algebra, 1997. doi:10.1137/1.9781611971446.

[45] S. Valadez-Godínez, H. Sossa, R. Santiago-Montero, On the accuracy and computational cost of spiking neuron implementation, Neural Networks (2020). doi:10.1016/j.neunet.2019.09.026.

[46] E. Bedrosian, A product theorem for hilbert transforms, Proceedings of the IEEE 51 (1963). doi:10.1109/PROC.1963.2308.

[47] J. Vohryzek, G. Deco, B. Cessac, M. L. Kringelbach, J. Cabral, Ghost attractors in spontaneous brain activity: Recurrent excursions into functionally-relevant bold phase-locking states, Frontiers in Systems Neuroscience 14 (2020). doi:10.3389/fnsys.2020.00020.

[48] M. Shanahan, Metastable chimera states in community-structured oscillator networks, Chaos: An Interdisciplinary Journal of Nonlinear Science 20 (2010) 013108. doi:10.1063/1.3305451.
URL https://aip.scitation.org/doi/abs/10.1063/1.3305451

[49] M. Wildie, M. Shanahan, Metastability and chimera states in modular delay and pulse-coupled oscillator networks, Chaos: An Interdisciplinary Journal of Nonlinear Science 22 (4) (2012) 043131.

[50] J. Cabral, E. Hugues, O. Sporns, G. Deco, Role of local network oscillations in resting-state functional connectivity, Neuroimage 57 (1) (2011) 130–139.

[51] M. Saggar, O. Sporns, J. Gonzalez-Castillo, P. A. Bandettini, G. Carlsson, G. Glover, A. L. Reiss, Towards a new approach to reveal dynamical organization of the brain using topological data analysis, Nature Communications 9 (2018). doi:10.1038/s41467-018-03664-4.

[52] M. Nicolau, A. J. Levine, G. Carlsson, Topology based data analysis identifies a subgroup of breast cancers with a unique mutational profile and excellent survival, Proceedings of the National Academy of Sciences of the United States of America 108 (2011) 7265–7270. doi:10.1073/PNAS.1102826108/SUPPL_FILE/PNAS.201102826SI.PDF.
URL https://www.pnas.org/doi/abs/10.1073/pnas.1102826108

[53] J. Meriam, Dynamics, Wiley, USA, 1971.

[54] T. A. Welch, A technique for high-performance data compression, Computer 17 (1984). doi:10.1109/MC.1984.1659158.

[55] J. Ziv, A. Lempel, Compression of individual sequences via variable-rate coding, IEEE Transactions on Information Theory 24 (1978). doi:10.1109/TIT.1978.1055934.

[56] A. G. Casali, O. Gosseries, M. Rosanova, M. Boly, S. Sarasso, K. R. Casali, S. Casarotto, M. A. Bruno, S. Laureys, G. Tononi, M. Massimini, A theoretically based index of consciousness independent of sensory processing and behavior, Science Translational Medicine 5 (8 2013). doi:10.1126/SCITRANSLMED.3006294/SUPPL_FILE/5-198RA105_SM.PDF.
URL https://www.science.org/doi/abs/10.1126/scitranslmed.3006294

[57] P. Sengupta, The laboratory rat: Relating its age with human's, International Journal of Preventive Medicine 4 (2013).

[58] C. F. Beckmann, S. M. Smith, Tensorial extensions of independent component analysis for multisubject fmri analysis, Neuroimage 25 (1) (2005) 294–311.

[59] E. DuPre, T. Salo, Z. Ahmed, P. A. Bandettini, K. L. Bottenhorn, C. Caballero-Gaudes, L. T. Dowdle, J. Gonzalez-Castillo, S. Heunis, P. Kundu, et al., Te-dependent analysis of multi-echo fmri with* tedana, Journal of Open Source Software 6 (66) (2021) 3669.

[60] E. A. Papp, T. B. Leergaard, E. Calabrese, G. A. Johnson, J. G. Bjaalie, Waxholm space atlas of the sprague dawley rat brain, NeuroImage 97 (2014). doi:10.1016/j.neuroimage.2014.04.001.

[61] P. A. Valdés-Hernández, A. Sumiyoshi, H. Nonaka, R. Haga, E. Aubert-Vásquez, T. Ogawa, Y. Iturria-Medina, J. J. Riera, R. Kawashima, An in vivo mri template set for morphometry, tissue segmentation, and fmri localization in rats, Frontiers in Neuroinformatics 5 (2011). doi:10.3389/fninf.2011.00026.

[62] P. Expert, S. D. Nigris, T. Takaguchi, R. Lambiotte, Graph spectral characterization of the xy model on complex networks, Physical Review E 96 (2017). doi:10.1103/PhysRevE.96.012312.

[63] A. Escrichs, C. Biarnes, J. Garre-Olmo, J. M. Fernández-Real, R. Ramos, R. Pamplona, R. Brugada, J. Serena, L. Ramió-Torrentà, G. Coll-De-Tuero, L. Gallart, J. Barretina, J. C. Vilanova, J. Mayneris-Perxachs, M. Essig, C. R. Figley, S. Pedraza, J. Puig, G. Deco, Whole-brain dynamics in aging: Disruptions in functional connectivity and the role of the rich club, Cerebral Cortex 31 (2021). doi:10.1093/cercor/bhaa367.

[64] A. R. McIntosh, V. Vakorin, N. Kovacevic, H. Wang, A. Diaconescu, A. B. Protzner, Spatiotemporal Dependency of Age-Related Changes in Brain Signal Variability, Cerebral Cortex (New York, NY) 24 (7) (2014) 1806–1817. doi:10.1093/cercor/bht030.
URL https://www.ncbi.nlm.nih.gov/pmc/articles/PMC4051893/

[65] A. R. McIntosh, Neurocognitive Aging and Brain Signal Complexity, iSBN: 9780190236557 (Feb. 2019). doi:10.1093/acrefore/9780190236557.013.386.
URL https://

[66] V. Müller, U. Lindenberger, Lifespan differences in nonlinear dynamics during rest and auditory oddball performance, Developmental Science 15 (4) (2012) 540–556, _eprint: https://onlinelibrary.wiley.com/doi/pdf/10.1111/j.1467-7687.2012.01153.x. doi:10.1111/j.1467-7687.2012.01153.x.
URL https://onlinelibrary.wiley.com/doi/abs/10.1111/j.1467-7687.2012.01153.x